High-Voltage MEMS Plasma Switch for Boosting the Energy Transfer Efficiency in Triboelectric Nanogenerators

Hemin Zhang, Frederic Marty, Dimitri Galayko, Naida Hodzic, Philippe Basset

HIGH-VOLTAGE MEMS PLASMA SWITCH FOR BOOSTING THE ENERGY TRANSFER EFFICIENCY IN TRIBOELECTRIC NANOGENERATORS

Hemin Zhang[1,2], Frédéric Marty[1], Dimitri Galayko[3], Naida Hodzic[1] and Philippe Basset[1]
[1] Université Paris-Est, ESYCOM, ESIEE Paris, 93162 Noisy-le-Grand Cedex, France
[2] University of Cambridge, Department of Engineering, Cambridge, United Kingdom
[3] Sorbonne Universités, LIP6, France

ABSTRACT

This paper presents for the first time a high-voltage MEMS plasma switch for boosting the energy transfer efficiency of conditioning circuits for triboelectric nanogenerators (TENGs). The novel MEMS switch has a narrow-hysteresis loop for a permanent high-efficiency energy conversion thanks to the combination of electrostatic actuation and plasma-discharge. At the same time, the converted energy is automatically transferred to a low-voltage reservoir through a buck converter. The experimental results show that the MEMS switch improves the harvesting efficiency by two orders of magnitude (145 times) compared to the conventional full-wave rectifying circuit architecture.

KEYWORDS

Electrostatic switch, triboelectric nanogenerator, high voltage, self-actuated, hysteresis, buck converter

INTRODUCTION

Triboelectric nanogenerators (TENGs) have attracted great research interests thanks to the characteristics of flexibility, simplicity and high output power density [1-3]. TENGs transfer the mechanical energy into electricity by coupling the principles of contact electrification and electrostatic induction [4]. For the most classical TENG, i.e. the contact-separate ones, opposite charges will be left on the surfaces of the two contact materials and a current will take place from one electrode to another to rebalance the electrostatic field when they separate/contact each other with the mechanical force.

How to efficiently manage the generated high peak voltages (above 100V) of the TENGs is still under consideration. It has recently been proved that adding switches [5-10] to the condition circuit could significantly improve the performances. For example, *Niu et al.* proposed a 2-stage circuit, which included a full-wave rectifier and a impedance-matched capacitance as the 1st stage, an *electronic switch* and a transformer as well as a storage reservoir as the 2nd stage for lowering down the high rectified DC voltage [5]. *Zi et al.* has reported that a *mechanical switch* synchronized with the movement of the TENG can improve the maximum energy-storage efficiency by up to 50% and promote the saturation voltage by at least a factor of two [6]. However, the energy consumption of the electrostatic switch is huge and the mechanical switch is not universal to all of the TENGs. We have previously reported a manually-fabricated electrostatic switch [9-10], which realized self-sustainability and hysteresis-loop.

In this paper, in order to further improve the stability and precision of the switch, we employ MEMS technique to fabricate the switch. It combines the principles of plasma discharge and electrostatic actuation. Narrow- and full-hysteresis loops can be generated by controlling the gap between anode and cathode.

DESIGN AND ANALYSIS

Systematic Diagram

A progressive contact-separate TENG [11] based on macro-shaped conductive polyurethane foam and polytetrafluoroethylene (PTFE) film was employed in the system. The conditioning circuit as shown in Fig. 1 includes a TENG and a Bennet doubler [12] to charge a small buffer capacitor as the 1st stage, and a buck converter for lowering down the voltage as the 2nd stage. Finally, a commercial regulator is used to stand the output voltage at 3.3V.

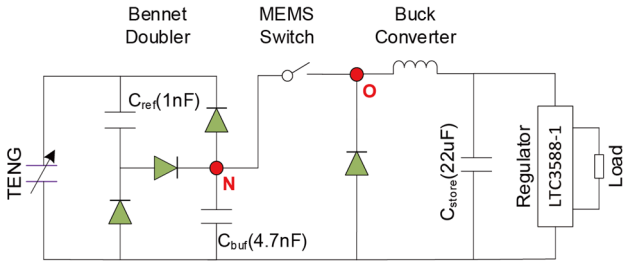

Fig. 1. The schematic of the 2-stage conditioning circuit for the TENG.

The small buffer capacitor (4.7nF) is firstly charged to a high voltage (hundreds of volts) through a Bennet topological circuit. As a special characteristic of the Bennet circuit, there is no voltage saturation phenomenon like the classical full-wave or half-wave rectifiers. On the contrary, the voltage across C_{buf} will increase exponentially until it approaches the voltage limitation of the capacitors or of the diodes. Thus V_{Cbuf} can approach a very high value.

When V_{Cbuf} reaches the ON voltage of the switch, the switch will be actuated ON and then the energy in C_{buf} will be transferred to the storage capacitor C_{store} (22µF) through the buck converter. As a result, V_{Cbuf} decreases until it reaches the OFF voltage of the switch. There are two cases for the switch to operate: i) a full-hysteresis loop, indicating a high ON voltage (hundreds of volts) and a very low OFF voltage (close to 0V); ii) a narrow-hysteresis loop, having also a high ON voltage, but an OFF voltage only a few percents lower than the ON voltage. A schematic of the two hysteresis loops can be found in Fig. 2. Theoretically, a narrow-hysteresis switch brings a higher energy harvesting efficiency because the circuit can always

operate at the optimized point having the highest energy per cycle.

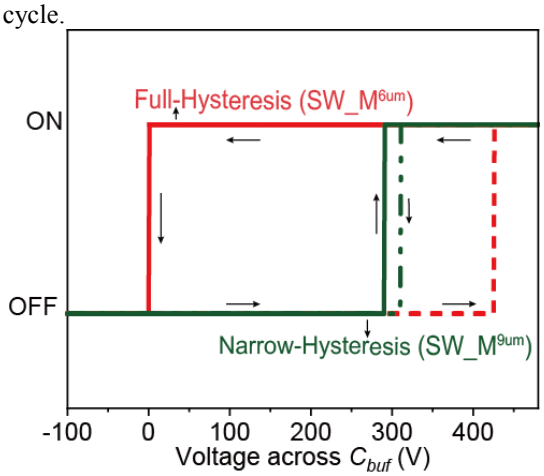

Fig. 2. The schematic of the ON/OFF statuses of the switch with a full- or a narrow- hysteresis loop. Dashed lines indicate the voltage upward curves while the solid lines show the voltage downward curves.

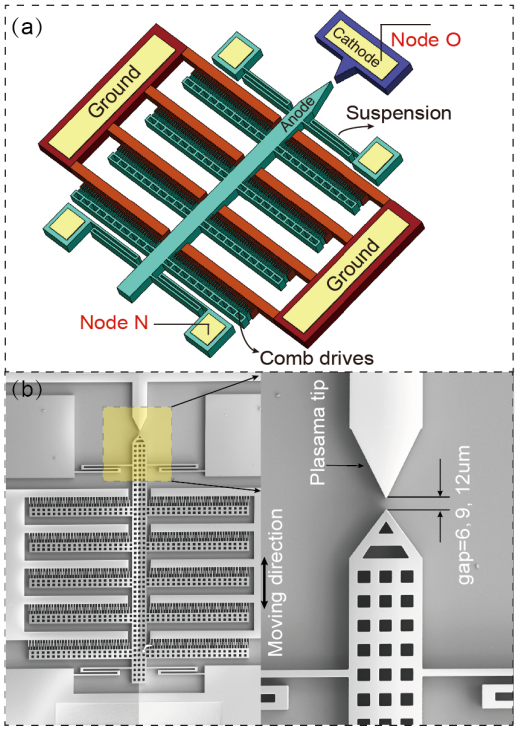

Fig. 3. The schematic (a) and SEM image (b) of the plasma switch.

Switch Design and Analysis

A schematic of the switch is shown in Fig. 3(a). A fixed electrode as cathode is connected to Node O (referred in Fig. 1), i.e. the input of the buck converter. A movable electrode as anode is connected to Node N (referred in Fig. 1), i.e. the output of the Bennet. Four suspension beams support the movement of the anode, which is obtained with four electrostatic comb-drives actuators connected to the reference ground.

When a high voltage is applied between the anode and the ground, it pulls the anode close to the cathode. Thanks to the specific design, there is no pull-in occurring in any situation because the anode and cathode electrodes work like a pair of stoppers: before the voltage across the comb-fingers reaches the pull-in, physical contact always arises first between the anode and cathode electrodes, which results in the release the energy and drop of the voltage.

As the switch combines the principles of electrostatic actuation and plasma discharge, the foresaid two cases of hysteresis loop can be realized. The full-hysteresis is attributed to the electrostatic actuation resulting in a direct physical contact between anode and cathode. The narrow-hysteresis is due to the plasma discharge when the applied voltage is high enough to reach the air breakdown voltage but not enough for the physical contact, whose threshold voltage is based on the Paschen's law curve [13]. Our device works in the air (a constant pressure), therefore the gap between anode and cathode becomes the critical parameter that determines the final breakdown voltage. The gap (g) between anode and cathode is dynamically changing with the variation of the applied voltage, therefore the breakdown voltage of the device will change as well, according to the Paschen's law:

$$V_b = \frac{Bpg}{ln(Apg) - ln(ln(\frac{1}{\gamma_i} + 1))} \quad (1)$$

where g is the dynamic gap between anode and cathode, and here is initially designed as 6μm, 9μm, and 12μm; p is the operating pressure; γ_i is the gas composition and A and B are constants based on the gas composition. The Paschen's law curve as well as the function curve of the voltage (V_{Cbuf}) versus the fingers' displacement are shown in Fig. 4.

It can be concluded that in case the gap g is small, the breakdown voltage would be ultra-high thus physical contact occurs before plasma discharge, and a full-hysteresis switch is obtained. When the gap g is high enough so that the voltage limit for physical contact is much higher than that of the breakdown, the plasma discharge takes place first and a narrow-hysteresis loop is expected as the current of the plasma discharge is much lower than that of the physical contact.

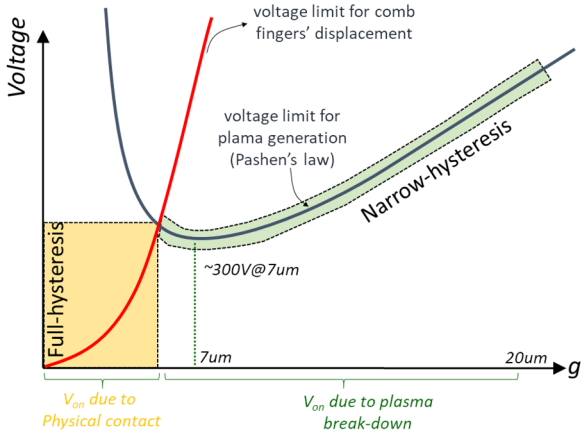

Fig. 4. The Paschen's las curve and the function of V_{ON} versus the gap between anode and cathode.

Fabrication Process

The fabrication of the switch is based on a dicing-free silicon-on-insulator (SOI) technique. The SOI wafer used in our fabrication has a 40μm device layer, a 2μm box layer

and a 400μm handle layer. The SEM image can be found in Fig. 3(b). The fabrication process is shown in Fig. 5 and the illustrations of the process steps are as follows:

a) Photolithography for front-side DRIE and pads opening
b) Front DRIE for the pads opening
c) Remove photoresist and aluminium sputtering (1μm)
d) Remove the backside oxidation using buffered oxide etching
e) Backside aluminum sputtering (0.5μm)
f) Front DRIE etching until the box layer
g) Backside DRIE etching until the box layer
h) Vapour HF release

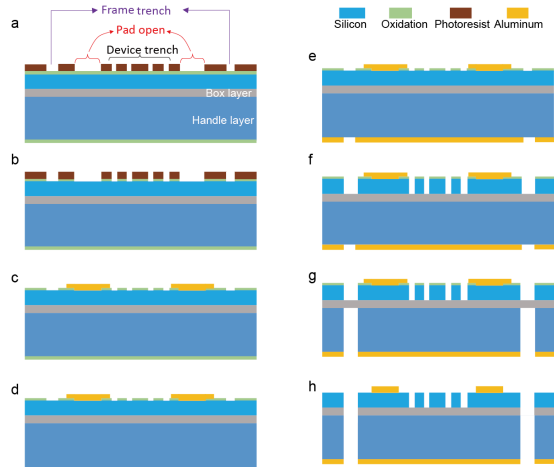

Fig. 5. The fabrication process of the switch.

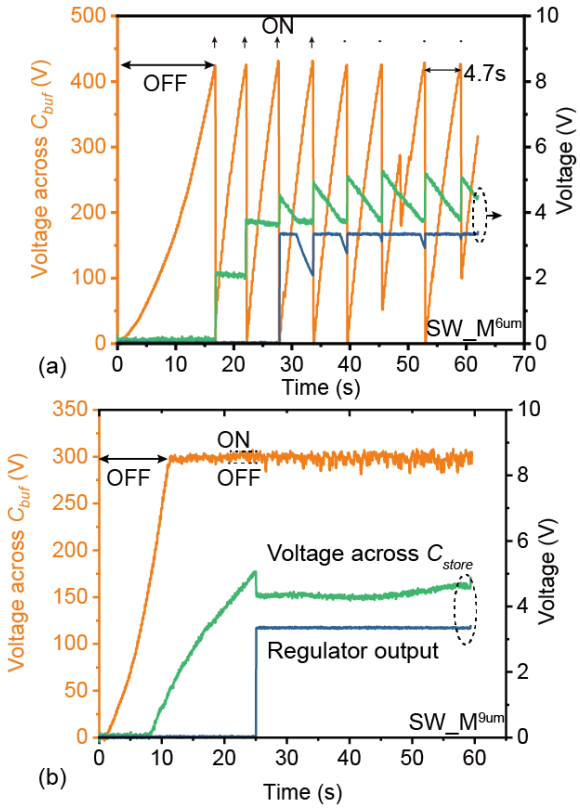

Fig. 6. Voltage across the buffer capacitor (C_{buf}), across the storage capacitor (C_{store}), and at the regulator output when using switches with 6μm-gap ($SW\_M^{6\mu m}$, a) and 9μm-gap ($SW\_M^{9\mu m}$, b).

EXPERIMENTAL RESULTS

We firstly did the experiments with the conditioning circuit shown in Fig. 1 to test the effectiveness of the whole system. When using a switch with $g = 6\mu m$ in the circuit, a full-hysteresis is obtained: the switch turns ON at a high-voltage (~425V) and turns OFF at 0V, as the orange line shows in Fig. 6(a), which indicates a hysteresis loop of ~425V. The recharging time from 0V to the ON-voltage is 4.7s and the switch-ON period is 0.2s. Thus the ON-OFF frequency for the switch ($g = 6\mu m$) is ~0.2Hz. However, if applying the regulator and a resistive load of 660kΩ, the output of the regulator cannot stand at 3.3V continuously because of the long recharging time.

In contrast, when using a switch with $g = 9\mu m$, there is a small ON-OFF hysteresis loop (<10V), as shown in Fig. 6(b). The narrow hysteresis results in a higher ON/OFF frequency of ~1.7Hz. Despite the ON voltage of 300V much lower than that using $SW\_M^{6\mu m}$, the output of the regulator can always stand at 3.3V with a load of 660kΩ. The equivalent available RMS power that can be applied to a load is $P_M = V^2/R = 15\mu W$.

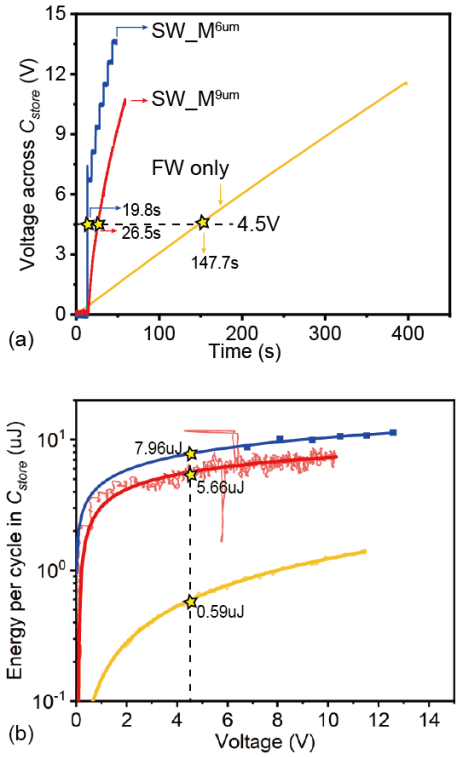

Fig. 7. The charging curves of the storage capacitor with three different methods (a). FW only here means we use the basic full-wave rectifier to directly charge a 22uF capacitor. The periods to get 4.5V for the three methods are 19.8s, 26.5s and 147.7s, respectively. Energy per cycle versus voltage across C_{store} without applying any load and the regulator (b).

The following experiments were done to compare the efficiencies of different circuits and switches for charging a 22μF capacitor. Performances of the circuits with Bennet and switches (both $SW\_M^{6\mu m}$ and $SW\_M^{9\mu m}$) as well as the most basic circuit of full-wave are compared. The charging curves and energy per cycle in C_{store} versus voltages without

applying regulators nor loads are drawn in Fig. 7(a) and 7(b). It can be seen that the periods to charge the capacitor to 4.5V are 19.8s, 26.5s and 147.7s for the three circuits, respectively. Also, the energy per cycle at the voltage of 4.5V for the three circuits are 7.96μJ/cycle, 5.66μJ/cycle and 0.59μJ/cycle, respectively. If we define the charging efficiency as the energy per cycle in C_{store} at 4.5V (the regulator's operation voltage) divided by the charging period to this voltage, we can conclude that using the 2-stage conditioning circuit with a 6μm-gap MEMS switch improves the energy transfer efficiency by 145 times (7.96μJ/cycle/19.8s versus 0.59μJ/cycle/147.7s) compared to only using full-wave rectifier.

CONCLUSIONS

In summary, this paper proposed and fabricated a MEMS switch using the principles of electrostatic actuation and plasma discharge to significantly improve the energy harvesting efficiency. The proposed switch can be employed in a wider energy harvesting area like the electret kinetic energy harvesters (eKEH) by adjusting the ON/OFF voltage of the switch by proper designs.

REFERENCES

[1]. J. Chen, Z. L. Wang, "Reviving vibration energy harvesting and self-powered sensing by a triboelectric nanogenerator." *Joule*., vol. 1, no. 3, pp. 480-521, Nov. 2017

[2]. K. Tao, H. Yi, Y. Yang, H. Chang, J. Wu, L. Tang, Z. Yang, N. Wang, L. Hu, Y. Fu, J. Miao, "Origami-inspired electret-based triboelectric generator for biomechanical and ocean wave energy harvesting." *Nano Energy*. doi.org/10.1016/j.nanoen.2019.10419. Oct. 2019.

[3]. R. Hinchet, H. J. Yoon, H. Ryu, M. K. Kim, E. K. Choi, D. S. Kim, S. W. Kim, "Transcutaneous ultrasound energy harvesting using capacitive triboelectric technology." *Science,* vol. 365, no. 6452, pp. 491-4, Aug. 2019.

[4]. A. Ghaffarinejad, J. Y. Hasani, R. Hinchet, Y. Lu, H. Zhang, A. Karami, D. Galayko, S. W. Kim, P. Basset "A conditioning circuit with exponential enhancement of output energy for triboelectric nanogenerator". *Nano Energy*. vol. 51, pp. 173-84, Sep. 2018.

[5]. S. Niu, X. Wang, F. Yi, Y. S. Zhou, Z. L. Wang, "A universal self-charging system driven by random biomechanical energy for sustainable operation of mobile electronics". *Nature Communications*., vol. 11, no. 6, pp. 8975, Dec. 2015.

[6]. Y. Zi, J. Wang, S. Wang, S. Li, Z. Wen, H. Guo, Z. L. Wang, "Effective energy storage from a triboelectric nanogenerator." *Nature Communications*., vol. 11, no. 7, pp. 10987, Mar. 2016.

[7]. J. Yang, F. Yang, L. Zhao, W. Shang, H. Qin, S. Wang, X. Jiang, G. Cheng, Z. Du, "Managing and optimizing the output performances of a triboelectric nanogenerator by a self-powered electrostatic vibrator switch." *Nano Energy.*, vol. 1, no. 46, pp. 220-8, Apr. 2018.

[8]. G. Cheng, H. Zheng, F. Yang, L. Zhao, M. Zheng, J. Yang, H. Qin, Z. Du, Z. L. Wang, "Managing and maximizing the output power of a triboelectric nanogenerator by controlled tip–electrode air-discharging and application for UV sensing." *Nano Energy*., vol. 1, no. 44, pp. 208-16, Feb. 2018.

[9]. H. Zhang, D. Galayko, P. Basset, "A self-sustained energy storage system with an electrostatic automatic switch and a buck converter for triboelectric nanogenerators", Proc. of PowerMEMS'18, USA, Dec. 2018.

[10]. H. Zhang, G. Dimitri, and P. Basset, "A conditioning system for high-voltage electrostatic/triboelectric energy harvesters using Bennet doubler and self-actuated hysteresis switch", The 20th International Conference on Solid-State Sensors, Actuators and Microsystems (TRANSDUCERS'19), June 2019.

[11]. H. Zhang, Y. Lu, A. Ghaffarinejad, P. Basset, "Progressive contact-separate triboelectric nanogenerator based on conductive polyurethane foam regulated with a Bennet doubler conditioning circuit". *Nano energy*. vol. 51, pp. 10-8, Sep. 2018.

[12]. A. Karami, D. Galayko and P. Basset, "Series-parallel charge pump conditioning circuits for electrostatic kinetic energy harvesting", *IEEE Transactions on Circuits and Systems I: Regular Papers*, vol. 64, no. 1, pp. 227 – 240, 2017.

[13]. T. Ono, D. Y. Sim, M. Esashi, "Micro-discharge and electric breakdown in a micro-gap." *Journal of Micromechanics and Microengineering.*, vol. 10, no. 3, pp. 445, Sep. 2000.

CONTACT

*H. Zhang, Email: 1989hemin@gmail.com